Title
Probing the localized to itinerant behavior of the 4f electron in CeIn3−xSnx by Gd3+ electron spin resonance

Journal
Physical Review B, 86(12)

ISSN
2469-9950

Authors
Bittar, EM
Adriano, C
Giles, C
et al.

Publication Date
2012-09-15

DOI
10.1103/physrevb.86.125108

Probing the localized to itinerant behavior of the 4f electron in $CeIn_{3-x}Sn_x$ by Gd^{3+} electron spin resonance

E. M. Bittar,[1,2,*] C. Adriano,[1] C. Giles,[1] C. Rettori,[1,3] Z. Fisk,[4] and P. G. Pagliuso[1,4]

[1]*Instituto de Física "Gleb Wataghin," UNICAMP, 13083-859 Campinas, SP, Brazil*

[2]*Laboratório Nacional de Luz Síncrotron, C.P. 6192, 13083-970 Campinas, SP, Brazil*

[3]*Centro de Ciências Naturais e Humanas, Universidade Federal do ABC, 09210-170 Santo André, SP, Brazil*

[4]*Department of Physics and Astronomy, University of California, Irvine, Irvine, California 92697-4575, USA*

(Received 4 October 2011; revised manuscript received 24 July 2012; published 6 September 2012)

The $CeIn_{3-x}Sn_x$ cubic heavy fermion system presents an antiferromagnetic transition at $T_N = 10$ K, for $x = 0$, that decreases continuously down to 0 K upon Sn substitution at a critical concentration of $x_c \approx 0.65$. In the vicinity of $T_N \to 0$ the system shows non-Fermi liquid behavior due to antiferromagnetic critical fluctuations. For a high Sn content, $x \gtrsim 2.2$, intermediate valence effects are present. In this work we show that Gd^{3+}-doped electron spin resonance (ESR) probes a change in the character of the Ce 4f electron, as a function of Sn substitution. The Gd^{3+} ESR results indicate a transition of the Ce 4f spin behavior from localized to itinerant. Near the quantum critical point, on the antiferromagnetic side of the magnetic phase diagram, both localized and itinerant behaviors coexist.

DOI: 10.1103/PhysRevB.86.125108 PACS number(s): 71.27.+a, 74.40.Kb, 76.30.−v

I. INDRODUCTION

Heavy fermion (HF) systems have shown to the scientific community interesting physical phenomena like antiferromagnetism (AFM), superconductivity (SC),[1] and non-Fermi liquid (NFL) behavior in the vicinity of quantum instabilities.[2] However, the evolution from high-temperature unscreened localized f electrons to itinerant heavy quasiparticles at low temperature is still an open question in condensed matter physics. The description of these HF materials stands on the Kondo lattice model,[1] in which there are three important energy scales: the crystalline electric field (CEF) splitting, the characteristic temperature T^*, and the single impurity Kondo temperature T_K. The latter is related to the screening of local moments by the conduction electrons due to the Kondo effect, whereas T^* represents the crossover between a lattice of Kondo impurities and a coherence state where the hybridization becomes a global process. This energy scale is related to the Ruderman-Kittel-Kasuya-Yosida (RKKY) exchange interaction, since it corresponds to the nearest-neighbor intersite coupling, which is mediated by conduction electrons.[3]

The cubic HF $CeIn_{3-x}Sn_x$ system is an interesting series for studying the correlations between T_K and T^*. For $x = 0$ the compound is AFM with $T_N = 10$ K, and by Sn substitution, T_N decreases continuously down to 0 K at a critical concentration $x_c \approx 0.65$.[4,5] This system resembles the behavior of $CeIn_3$ under pressure, where an SC state emerges at a critical pressure $P_c \approx 25$ kbar with a critical temperature $T_c \approx 0.15$ K as $T_N \to 0$.[6] In the vicinity of P_c and x_c both systems show NFL behavior, suggesting that AFM critical fluctuations are present. Recently, an analysis of the magnetic contribution to the specific heat in $CeIn_3$ showed that the magnetic fluctuations in this material are effectively 2D.[7] Indeed, an almost-linear dependence of $T_N(x)$ is seen for $CeIn_{3-x}Sn_x$,[5] in contrast to what is predicted by the 3D spin density wave (SDW) theory and it cannot be associated with disorder effects.[8] The reported scenario for the pressure and Sn substitution driven quantum critical point (QCP) were different. For $CeIn_{3-x}Sn_x$ an SDW description of criticality based on critical exponents analysis of a 3D AFM was used.[8,9] In the SDW QCP the 4f moments are delocalized in the AFM state and no change in the Fermi surface is observed across the QCP.[2] However, in a local class of QCP the 4f electrons remain localized in the magnetically ordered phase and there is an abrupt change in the Fermi surface volume at the QCP.[2] For $CeIn_3$ under pressure a local QCP was proposed due to a Fermi surface volume change observed in de Haas–van Alphen measurements.[10] Also, some indication of a first-order quantum phase transition instead of a QCP was reported by nuclear quadrupolar resonance measurements carried out around P_c.[11]

In this work we study the evolution of the Gd^{3+} electron spin resonance (ESR) signal in the $CeIn_{3-x}Sn_x$ system through its QCP. Since the Ce^{3+} ESR signal is silent, we chose Gd^{3+} as a probe because it is almost a pure S-state, so its total angular momentum is mainly due to spin, being weakly perturbed by CEF effects. To the best of our knowledge no systematic reports on microscopic studies on the Sn substitution x_c were reported. Our Gd^{3+} ESR results show a change in the character of the Ce 4f electron, as a function of Sn substitution, which indicates a transition from localized to itinerant behavior. Near the QCP ($x = 0.5$), on the AFM side of the magnetic phase diagram,[5,8] the Ce 4f spin present simultaneously both localized and itinerant characters.

II. EXPERIMENTAL DETAILS

Single crystals of Gd doped $CeIn_{3-x}Sn_x$ are synthesized by the flux-growth technique. Elemental Ce:Gd:In:Sn are weighted at the ratio $1-y{:}y{:}10-(10x/3){:}10x/3$, with a nominal value for y of 0.005 and $x = 0$, 1.5, and 3. Polycrystalline samples are also grown by arc melting in an argon atmosphere. In this case the reactants ratio used is $1-y{:}y{:}3-x{:}x$, with the same nominal value for y and $x = 0$, 0.5, 0.7, 1.5, and 3. X-ray powder diffraction measurements confirm the cubic $AuCu_3$ (Pm-$3m$)–type structure for all synthesized compounds. The temperature dependence of the magnetic

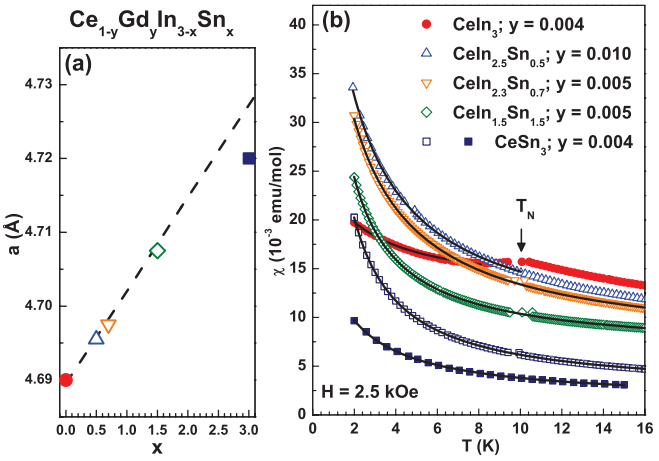

FIG. 1. (Color online) Gd^{3+} in $Ce_{1-y}Gd_yIn_{3-x}Sn_x$. (a) Cubic lattice parameter a dependance as a function of x. The dashed line represents the Vegard law.[5] For $x = 3$ the departure of linear behavior is due to the Ce ion intermediate valence effects for $x \gtrsim 2.2$.[4] (b) Low-temperature dependence of $\chi(T)$ at $H = 2.5$ kOe. Solid lines are the Curie-Weiss fitting. Filled symbols identify single-crystalline samples; open circles, polycrystals.

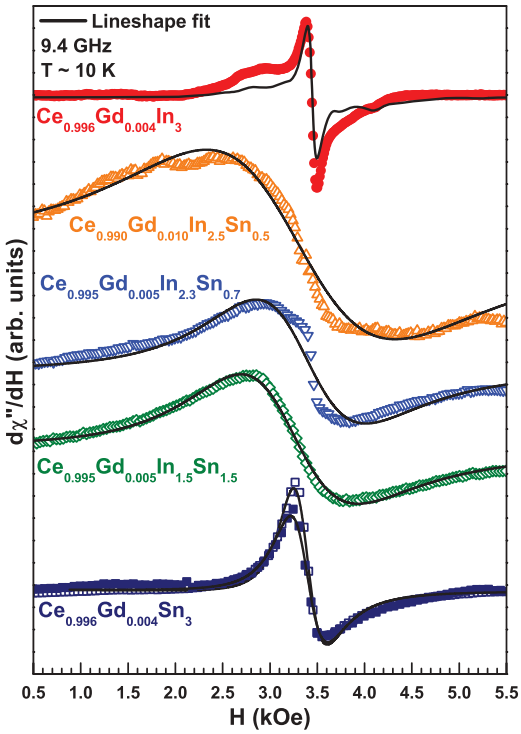

FIG. 2. (Color online) Gd^{3+} ESR powder spectra in $Ce_{1-y}Gd_yIn_{3-x}Sn_x$ for $y \sim 0.5\%$, at $T \approx 10$ K, emphasizing the resonance region. Solid lines are the single Dysonian line-shape analysis. For $Ce_{0.996}Gd_{0.004}In_3$ the spin Hamiltonian model discussed in Ref. 14 for powder was used.[15] Background contribution is present for the $x = 0.5$ and $x = 0.7$ samples (see text). Filled symbols identify single-crystalline samples; open circles, polycrystals.

susceptibility, $\chi(T)$, is measured for $2 \leqslant T \leqslant 300$ K, after zero-field cooling. All ESR experiments are performed on a fine powder ($d \leqslant 38$ μm) in a Bruker ELEXSYS X-band spectrometer (9.4 GHz) with a TE_{102} cavity coupled to a helium-gas-flux temperature controller system at $4.2 \leqslant T \leqslant 300$ K. Fine powder of crushed single and polycrystals are used in the ESR experiments in order to increase the ESR signal-to-noise ratio. As reference compounds, Gd doped $LaIn_{3-x}Sn_x$ alloys were also grown and studied.[12]

III. EXPERIMENTAL RESULTS

The actual Sn concentrations are obtained from the cubic lattice parameter, which one expects to follow a linear increase (Vegard's law)[5] [see Fig. 1(a)]. For $x = 3$ the departure of linear behavior is due to the Ce ion intermediate valence effects for $x \gtrsim 2.2$.[4] The temperature dependence of the magnetic susceptibility $\chi(T)$ for the series of compounds $Ce_{1-y}Gd_yIn_{3-x}Sn_x$, corrected for the core diamagnetism, is shown in Fig. 1(b). From the Curie-Weiss law fitting of the low-temperature magnetic susceptibility data, the Gd doping concentration is obtained and its values are listed in Table I.

Figure 2 shows the ESR (X-band) powder spectra, at $T \sim 10$ K, of Gd^{3+} in $CeIn_{3-x}Sn_x$. Except for $x = 0$, the

TABLE I. Experimental parameters for Gd^{3+} diluted in $Ce_{1-y}Gd_yIn_{3-x}Sn_x$. Values of γ are taken from Ref. 5.

Gd^{3+} in	Gd y	Δg	ΔH_0 (Oe)	b (Oe/K)	γ (mJ/mol K^2)
$CeIn_3$	0.004	$-0.023(5)$	120(5)	0.1(1)	130
$CeIn_{2.5}Sn_{0.5}$	0.010	$+0.007(10)$	825(45)	38(3)	730(50)
$CeIn_{2.3}Sn_{0.7}$	0.005	$+0.027(10)$	820(25)	15(5)	750(50)
$CeIn_{1.5}Sn_{1.5}$	0.005	$+0.140(10)$	650(60)	30(5)	250(20)
$CeSn_3$	0.004	$+0.027(5)$	150(5)	16(1)	73

ESR spectra consist of a single Dysonian resonance, consistent with the ESR for localized magnetic moments in a metallic host with a skin depth smaller than the size of the used particles. By fitting the line shape to the appropriate admixture of absorption and dispersion Lorentzian derivatives, we obtain the g value and line width ΔH of the resonances. The solid lines are the best fit to the observed resonances and the obtained g shifts Δg [relative to the $g = 1.993(1)$ seen in cubic insulators] are presented in Table I. For Gd^{3+} in $CeIn_3$ the ESR spectrum shows the typical fine-structure features for powder samples,[13] with a main line at $H \sim 3.45$ kOe, associated with the $1/2 \leftrightarrow 1/2$ transition. A previous report on this compound, using the spin Hamiltonian $H = g\mu_B \mathbf{H} \cdot \mathbf{S} + (1/60)b_4(O_4^0 + 5O_4^4) + J_{fs}\mathbf{S} \cdot \mathbf{s}$,[14] extracted the crystal-field parameter $b_4 = 90(5)$ Oe.[15] For $Ce_{0.995}Gd_{0.005}In_{2.3}Sn_{0.7}$ a background line is present in the spectrum at $H \sim 3.4$ kOe and for $Ce_{0.99}Gd_{0.01}In_{2.5}Sn_{0.5}$ the ESR spectrum also shows some small contribution of the background. These background contributions are due to extrinsic impurities, with a resonance at $g \sim 2$, present in the cavity or in the cryostat quartz (even without any sample).

The temperature dependence of ΔH is shown in Fig. 3. For all samples there is a range where the width increases linearly with temperature. In this range the linear dependence of the ΔH is fitted to the expression $\Delta H - \Delta H_0 = bT$. The values for ΔH_0 (residual line width) and b (line-width thermal broadening) are presented in Table I and Fig. 4. The relatively

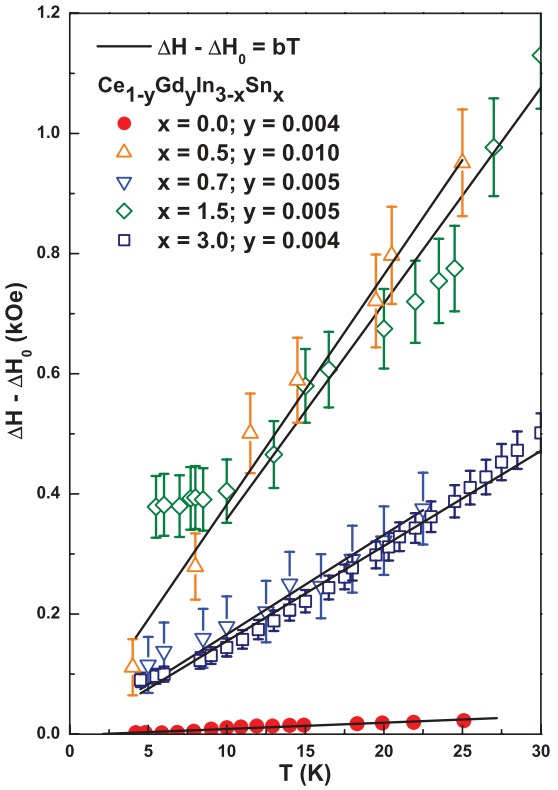

FIG. 3. (Color online) Temperature dependence of the Gd^{3+} ESR line width in $Ce_{1-y}Gd_yIn_{3-x}Sn_x$. Solid lines are the best fit to $\Delta H - \Delta H_0 = bT$. A deviation from the linear dependence of ΔH at low temperatures is seen for $x = 1.5$, which is related to short-range Gd-Gd interaction. Filled symbols identify single-crystalline samples; open circles, polycrystals.

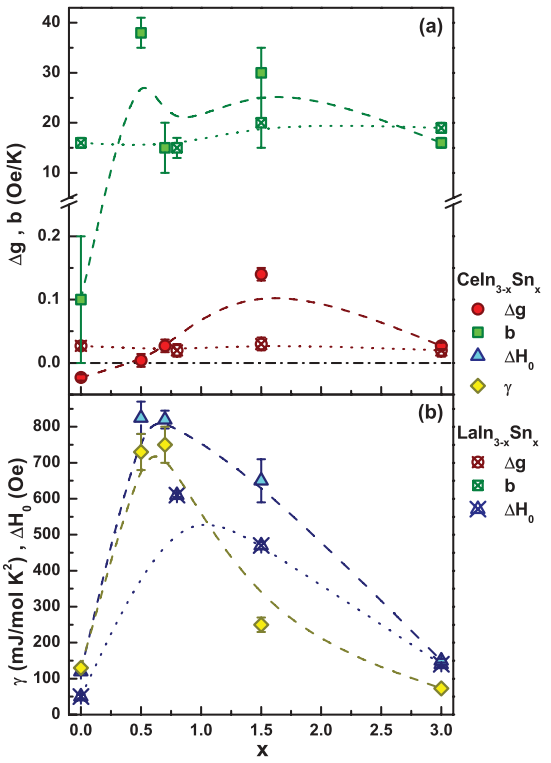

FIG. 4. (Color online) Gd^{3+} ESR in $Ce_{1-y}Gd_yIn_{3-x}Sn_x$. (a) Line-width thermal broadening b and g shift evolution. The dash-dotted line marks $\Delta g = 0$. (b) Sommerfeld coefficient γ and residual line-width ΔH_0 evolution. For comparison, the Gd^{3+} ESR in $La_{1-y}Gd_yIn_{3-x}Sn_x$ data are also shown.[12] Dashed and dotted spline lines are guides for the eye.

high ΔH_0 values for $0 < x < 3$ are probably due to unresolved CEF and disorder introduced by the In-Sn substitution. The ΔH_0 values follow the residual electrical resistivity ρ_0 behavior, since both are dependent on the disorder. One can see that ΔH_0 has the same pattern for $LaIn_{3-x}Sn_x$ [Fig. 4(b)], which follows the ρ_0 dependence (see Fig. 4 in Ref. 16). For $Ce_{0.996}Gd_{0.004}In_3$, only the ΔH temperature dependance of the main line is analyzed. A deviation from the linear dependence of ΔH at low temperature for $x = 1.5$ is related to short-range Gd-Gd interaction. Within the accuracy of the measurements, the g and b values are Gd concentration independent for $y < 1.0\%$ (not shown). Therefore, bottleneck and dynamic effects can be disregarded.[17]

Since in this work samples with different Sn content are grown by different methods, we show, particularly for $x = 3$ (Fig. 2), that there are no discernible differences in the ESR spectra of grounded single- vs polycrystalline samples. Hence, for the $CeIn_{3-x}Sn_x$ system, single and polycrystals are indistinguishable from the ESR point of view. However, this is not always the case in most systems and it cannot be established *a priori*. Table I and Fig. 4 do not distinguish single and polycrystalline samples.

The error bar values presented in Table I and Fig. 4 are determined by systematic measurements of different samples for most Sn concentrations and by analyzing the line-shape fitting for different field ranges. To exemplify such systematic procedures, Fig. 5 illustrates a line-shape analysis for different field range fittings, in this case for the $Ce_{0.990}Gd_{0.010}In_{2.5}Sn_{0.5}$ sample. One can observe that the slope of the line-width thermal broadening [Fig. 5(b)] and the g value [Fig. 5(c)] of the Gd^{3+} ESR are almost independent of the field range fitting. Also, Fig. 6 exemplifies different samples measurements for $Ce_{0.995}Gd_{0.005}In_{2.3}Sn_{0.7}$. Again, the b and g values [Fig. 6(b)] vary little between samples. Therefore, despite the large line width of the Gd^{3+} ESR in $Ce_{1-y}Gd_yIn_{3-x}Sn_x$, which would give rise to large error values, our systematic measurements and fitting procedures allow us to reduce the error and determine the values with a higher precision.

IV. ANALYSIS

A. Gd^{3+} ESR in metals

In metals, the exchange interaction $J_{fs}(q)\mathbf{S}\cdot\mathbf{s}$ between a Gd^{3+} localized $4f$ electron spin ($\mathbf{S}$) and the conduction electron spin ($\mathbf{s}$) of the host metal yields an ESR Δg (Knight shift) given by[18]

$$\Delta g = J_{fs}(0)\eta_{F_s}, \tag{1}$$

where $J_{fs}(0)$ is the effective exchange interaction parameter between the Gd^{3+} $4f$ local moment and the s-like conduction electrons in the absence of conduction electron momentum transfer ($q = |\mathbf{k} - \mathbf{k}'| = k_F[2(1 - cos\theta_{\mathbf{kk}'})]^{1/2} = 0$).[19] η_{F_s} is

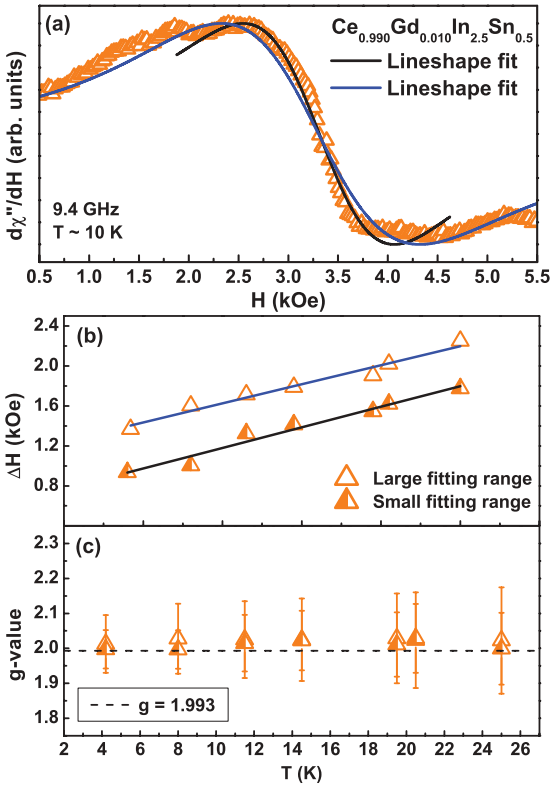

FIG. 5. (Color online) (a) Gd^{3+} ESR powder spectra in $Ce_{0.990}Gd_{0.010}In_{2.5}Sn_{0.5}$, at $T \approx 10$ K. Solid lines are the single Dysonian line-shape analysis for two field range fittings. (b) Temperature dependence of the Gd^{3+} ESR line width for the two field ranges shown in (a). Solid lines are the best fit to $\Delta H = \Delta H_0 + bT$. (c) g-value temperature dependence of the Gd^{3+} ESR for the two field ranges shown in (a). The dashed line is the g value for Gd^{3+} ESR in insulators.

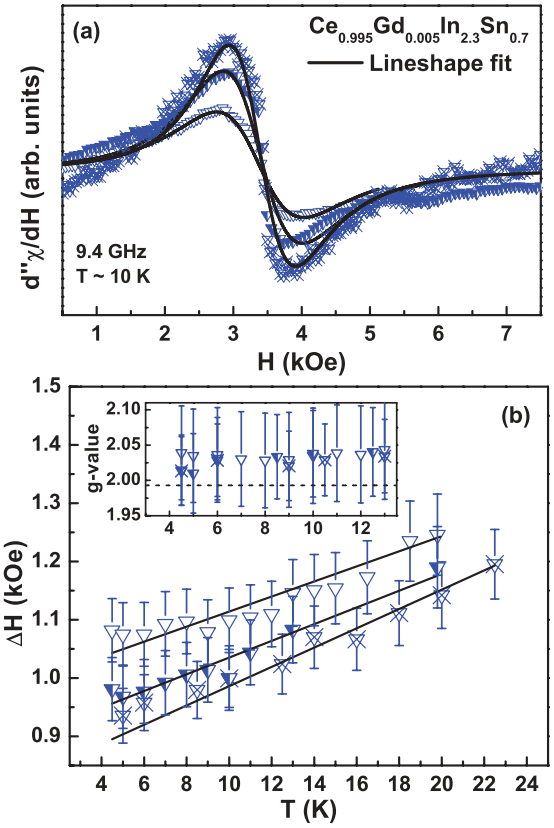

FIG. 6. (Color online) (a) Gd^{3+} ESR powder spectra in $Ce_{0.995}Gd_{0.005}In_{2.3}Sn_{0.7}$, at $T \approx 10$ K, for three samples with the same Sn concentration. Solid lines are the single Dysonian line-shape analysis. (b) Temperature dependence of the Gd^{3+} ESR line width for the three samples shown in (a). Solid lines are the best fit to $\Delta H = \Delta H_0 + bT$. Inset: Low-temperature g-value dependence of the Gd^{3+} ESR for the three samples shown in (a). The dashed line is the g value for Gd^{3+} ESR in insulators.

the s-like-band bare density of states for one spin direction at the Fermi surface.

In addition, the exchange interaction leads to a thermal broadening of ΔH, b (Korringa rate), given by[18]

$$b = \frac{d(\Delta H)}{dT} = \frac{\pi k_B}{g\mu_B} J_{fs}(0)^2 \eta_{F_s}^2, \tag{2}$$

where the constants k_B, μ_B, and g are the Boltzman constant, the Bohr magneton, and the Gd^{3+} g value in insulators ($g = 1.993$), respectively. The constant $\pi k_B/g\mu_B$ is 2.34×10^4 Oe/K in CGS units.

Equations (1) and (2) are normally used in the analysis of ESR data for noninteracting and highly diluted rare-earth magnetic moments in intermetallic compounds with appreciable residual resistivity, i.e., large conduction electrons spin-flip scattering (absence of "bottleneck" and "dynamic" effects).[17] Combining the above equations we can write

$$b = \frac{\pi k_B}{g\mu_B}(\Delta g)^2. \tag{3}$$

When the effective exchange interaction constant is not independent of the momentum transfer ($q \neq 0$), Eq. (2), in this more general case, has to be rewritten as

$$b = \frac{\pi k_B}{g\mu_B}\langle J_{fs}^2(q)\rangle \eta_{F_s}^2 \tag{4}$$

or, alternatively, using Eq. (1),

$$b = \frac{\pi k_B}{g\mu_B}\frac{\langle J_{fs}^2(q)\rangle_F}{J_{fs}^2(0)}\Delta g^2, \tag{5}$$

where $\langle J_{fs}^2(q)\rangle_F$ is the square of the effective exchange interaction parameter in the presence of conduction electron momentum transfer, averaged over the Fermi surface.[19]

One way to know if the system is momentum transfer dependent is to analyze Eq. (3). If the calculated Korringa rate b_{cal} by the experimental Δg is equal to the experimental Korringa rate b_{exp} ($b_{\text{cal}} = b_{\text{exp}}$), q dependance can be neglected. However, if $b_{\text{cal}} > b_{\text{exp}}$, then it cannot. This is because $\langle J_{fs}^2(q)\rangle_F / J_{fs}^2(0) \leqslant 1$, once $J(q)$ is proportional the Fourier transformation of $J(r)$, which amplitude decreases as a function of r. So the average $J(r)$ should be smaller than $J(0)$.

In cases where the conduction band also has d-, p-, or f-like electrons, Eqs. (1) and (2) are not valid and must be

rewritten, respectively, as

$$\Delta g = \Delta g_{fs} + \Delta g_{fd} + \Delta g_{fp} \ldots = J_{fs}(0)\eta_{F_s} + J_{fd}(0)\eta_{F_d} + J_{fp}(0)\eta_{F_p} + \ldots \quad (6)$$

and

$$b = \frac{\pi k_B}{g\mu_B}\left[F_s J_{fs}^2(0)\eta_{F_s}^2 + F_d J_{fd}^2(0)\eta_{F_d}^2 + F_p J_{fp}^2(0)\eta_{F_p}^2 + \ldots\right], \quad (7)$$

where $J_{fs}(0)$, $J_{fd}(0)$, and $J_{fp}(0)$ are the exchange interaction constants between the Gd^{3+} $4f$ spin and the s-, d-, and p-like bands, respectively. η_{F_s}, η_{F_d}, and η_{F_p} are the bare density of states for one spin direction at the Fermi surface for each respective band. $F_s = 1$, $F_d = 1/5$, and $F_p = 1/3$ are factors associated with the orbital degeneracy of the unsplit (no CEF effects) s, d, and p bands at the Fermi level, respectively.[20,21]

Multiband effects enhance the Korringa rate compared to $b_{\rm cal}$ [Eq. (3)], since the dependence of b is quadratic with the exchange interaction parameters, while for Δg it is linear and depends on the sign and strength of each exchange interaction constant. Therefore, the Δg sign can give valuable information about the interaction between the localized moment and its environment.

B. Gd^{3+} effective exchange interaction parameter calculations in $CeIn_{3-x}Sn_x$

We now analyze separately the experimental ESR data for each synthesized compound.

1. *Calculation for* $x = 0.0$

In the absence of strong electron-electron exchange interaction and assuming that $\langle J_{fs}^2(q)\rangle_F^{1/2} = J_{fs}(0)$, i.e., the effective exchange interaction is constant over the Fermi surface, one expects $b \approx 12(5)$ Oe/K from Eq. (3), using the experimental $\Delta g \simeq -23(5) \times 10^{-3}$. This value is much larger than that measured experimentally, $b = 0.1(1)$ Oe/K (Fig. 3). Thus, the approximations that the relaxation does not depend on q and that it is due to the contribution of a single conduction s-like band are not adequate. Since Δg is negative, a relaxation via a single s band is not plausible because $J_{fs}(0)$ is atomic-like and positive. Thus, for $\Delta g < 0$, contributions coming from covalent-like (negative) exchange interaction between the Gd^{3+} $4f$-electron and p or f bands must be taken into account in the relaxation process (multiband effects).[18] On the other hand, multiple bands would lead to a Korringa rate higher than the one expected from the Δg,[22] contrary to what is observed for Gd^{3+} in $CeIn_3$. Therefore, a strong q-dependent effective exchange interaction parameter $J_{fp}(q)$ or $J_{ff}(q)$ is expected in this compound. For $CeIn_3$ the local magnetic moment of Ce is compensated by the conduction electron sea due to the Kondo effect. However, when Gd^{3+} substitutes the Ce ions there is a strong Coulomb repulsion potential that decreases the local density of states at the Gd^{3+} site, hence decreasing the Korringa rate [Eq. (2) or (4)]. Theoretical calculations have already shown that the spin relaxation rate of a well-defined magnetic moment in the neighborhood of a fluctuating valence ion decreases in relation to the relaxation rate of an undoped metal.[23] Indeed, a much higher Korringa rate $b = 16(1)$ Oe/K was measured in Gd-doped $LaIn_3$.[15] This has also been observed for Gd in $CePd_3$ which presented an ESR ΔH thermal broadening five times smaller than in $LaPd_3$.[24] Besides, the observation of fine-structure features in the spectrum (Fig. 2) even up to room temperature without narrowing effects[18] (not shown) suggests a low local density of states at the Gd^{3+} site. Another consequence of the screening of the Ce^{3+} magnetic moment by conduction electrons is that the Gd^{3+} resonance does not sense the internal field caused by the AFM transition. No change in the relaxation or in the resonance field is observed below $T_N = 10$ K.

From the considerations above we can assume that the interaction of the Gd^{3+} $4f$ local moment is mainly with Ce f-like conduction electrons. We then can rewrite Eqs. (1) and (4), respectively, as

$$\Delta g = J_{ff}(0)\eta_{F_f} \quad (8)$$

and

$$b = \frac{\pi k_B}{g\mu_B} F_f \left\langle J_{ff}^2(q)\right\rangle_F \eta_{F_f}^2, \quad (9)$$

where $F_f = 1/7$ is associated with the orbital degeneracy of the unsplit f band at the Fermi level.[20,21]

In the free conduction electron gas model, the electronic heat capacity or Sommerfeld coefficient γ is given by

$$\gamma = (2/3)\pi^2 k_B^2 \eta_F \quad (10)$$

and one can obtain, using its experimental value, the bare density of states for one spin direction at the Fermi surface.

For $CeIn_3$ $\gamma^{x=0} = 130$ mJ/(mol K^2),[5] so we get from Eq. (10) $\eta_F^{x=0} = 28(2)$ states/(eV mol spin). Assuming that in this compound the density of states at the Fermi level for the $4f$ electrons $\eta_{F_f}^{x=0}$ is

$$\eta_{F_f}^{x=0} = \eta_F^{x=0} - \eta_F^{\rm LaIn_3},$$

where $\eta_F^{\rm LaIn_3} = 0.8(1)$ state/(eV mol spin) (see Fig. 4 in Ref. 25), we calculate $\eta_{F_f}^{x=0} = 27(2)$ states/(eV mol spin).

Using Eqs. (8) and (9), experimental values of Δg and b, and $\eta_{F_f}^{x=0} = 27(2)$ states/(eV mol spin), we obtain $J_{ff}(0) = -0.8(1)$ meV and $\langle J_{ff}^2(q)\rangle_F^{1/2} = 0.20(5)$ meV.

2. *Calculation for* $x = 0.5$

By substituting 16.67% of In by Sn, $x = 0.5$, T_N drops to $\sim$1.3 K,[5] very close to x_c. We also see Δg going from a relatively large negative to a very small, $\simeq 7(10) \times 10^{-3}$, positive value. From Eq. (3) we get $b_{\rm cal} \ll b_{\rm exp}$. It is clear that for $Ce_{0.990}Gd_{0.010}In_{2.50}Sn_{0.50}$ multiband effects are now present.[22] This is expected since Sn substitution led to the hybridization of the localized Ce^{3+} $4f$ electrons, turning them into an itinerant s-like conduction band. So, for $x = 0.5$ the Gd^{3+} resonance relaxes via the contribution of the Ce $4f$ itinerant s- and localized f-like bands. In this case, Eqs. (6) and (7) can be rewritten, respectively, as

$$\Delta g = J_{fs}\eta_{F_f^{it}} + J_{ff}\eta_{F_f^{\rm loc}} \quad (11)$$

and

$$b = \frac{\pi k_B}{g\mu_B}\left[J_{fs}^2\eta_{F_f^{it}}^2 + F_f J_{ff}^2 \eta_{F_f^{loc}}^2\right], \quad (12)$$

where $\eta_{F_f^{it}}$ and $\eta_{F_f^{loc}}$ are the band bare density of states for one spin direction at the Fermi surface for the itinerant- and localized-like $4f$ band, respectively.

From $\gamma^{x=0.5} = 730(50)$ mJ/(mol K^2)[5] and Eq. (10), we get $\eta_F^{x=0.5} = 155(2)$ states/(eV mol spin). Assuming that

$$\eta_{F_f}^{x=0.5} = \eta_F^{x=0.5} - \eta_F^{LaIn_{2.5}Sn_{0.5}},$$

where $\eta_F^{LaIn_{2.5}Sn_{0.5}} = 0.8(1)$ state/(eV mol spin) (see Fig. 4 in Ref. 25), we calculate $\eta_{F_f}^{x=0.5} = 154(2)$ states/(eV mol spin).

Solving the system of three equations below for $\eta_{F_f}^{x=0.5} = 154(2)$ states/(eV mol spin), $\Delta g \simeq 7(10)\times 10^{-3}$, $b = 38(3)$ Oe/K, and admitting that $J_{ff}^{x=0.5} = J_{ff}^{x=0} = 0.0008$ eV,

$$\eta_{F_f}^{x=0.5} = \eta_{F_f^{it}} + \eta_{F_f^{loc}} = 154,$$

$$\Delta g = J_{fs}\eta_{F_f^{it}} + 0.0008\eta_{F_f^{loc}} = 7\times 10^{-3},$$

and

$$b = 2.34\times 10^4\left[J_{fs}^2\eta_{F_f^{it}}^2 + \tfrac{1}{7}(0.0008)^2\eta_{F_f^{loc}}^2\right] = 38,$$

we obtain $J_{fs}(0) = 0.3(1)$ meV, $\eta_{F_f^{it}} = 115(10)$ states/(eV mol spin), and $\eta_{F_f^{loc}} = 40(5)$ states/(eV mol spin).

So, naively, this result indicates that a weight of 74% of the Ce f electrons becomes itinerant upon $x = 0.5$ Sn substitution, while the other 26% remains localized. One may argue that the multiband effects would in fact be due to the presence of s electrons arising from a weakened Kondo interaction at the Ce^{3+} site or by the addition of new electrons. However, small Sn substitution increases the conduction electron attractive potential[23] and does not profoundly change the density of states, as seen in $LaIn_{3-x}Sn_x$,[12,25] favoring the interpretation of a delocalization of the Ce f electrons.

3. *Calculation for x = 0.7*

For Gd^{3+} in $CeIn_{2.3}Sn_{0.7}$ the system is in the vicinity of the QCP and Eq. (3) predicts $b_{cal} \approx b_{exp}$. Therefore, we can consider a single s-like conduction band with no q dependance in the analysis of the resonance in this material. Hence, from $\gamma^{x=0.7} = 750(50)$ mJ/(mol K^2)[5] and Eq. (10), we get $\eta_F^{x=0.7} = 160(10)$ states/(eV mol spin). Using Eq. (2) we find $J_{fs}(0) = 0.2(1)$ meV, similar to the value found for $x = 0.5$.

4. *Calculation for x = 1.5*

The Δg value observed experimentally gives $b_{cal} \gg b_{exp}$ by Eq. (3). So, in this case q dependence is present and $\langle J_{fs}^2(q)\rangle_F^{1/2} \neq J_{fs}(0)$. From $\gamma^{x=1.5} = 250(20)$ mJ/(mol K^2)[5] and Eq. (10), we get $\eta_F^{x=1.5} = 53(4)$ states/(eV mol spin). Using Eqs. (1) and (4) we calculate $J_{fs}(0) = 2.6(2)$ meV and $\langle J_{fs}^2(q)\rangle_F^{1/2} = 0.7(1)$ meV, respectively.

5. *Calculation for x = 3.0*

From Eq. (3) we get $b_{cal} \approx b_{exp}$, i.e., multiband and q dependence effects of the exchange interaction may be neglected. Thus, from $\gamma^{x=3} = 73$ mJ/(mol K^2)[5] and Eq. (10) we get $\eta_F^{x=3} = 16(1)$ states/(eV mol spin). Using Eq. (2) we find $J_{fs}(0) = 1.7(1)$ meV.

TABLE II. Derived effective exchange interaction parameters for Gd^{3+} diluted in $CeIn_{3-x}Sn_x$.

Gd^{3+} in	$J_{fs}(0)$ (meV)	$\langle J_{fs}^2(q)\rangle_F^{1/2}$ (meV)	$\lvert J_{ff}(0)\rvert$ (meV)	$\langle J_{ff}^2(q)\rangle_F^{1/2}$ (meV)
$CeIn_3$			0.8(1)	0.20(5)
$CeIn_{2.5}Sn_{0.5}$	0.3(1)		0.8(1)	
$CeIn_{2.3}Sn_{0.7}$	0.2(1)			
$CeIn_{1.5}Sn_{1.5}$	2.6(2)	0.7(1)		
$CeSn_3$	1.7(1)			

C. Derived effective exchange interaction parametes summary

The derived effective exchange interaction parameters from the analysis above are summarized in Table II. Due to the suppositions and approximations considered in the calculations, the numerical values must be taken with care. However, it does not invalidate the qualitative microscopic description probed by ESR.

V. DISCUSSION

The nonmagnetic analog $LaIn_{3-x}Sn_x$ system is superconducting and shows Pauli paramagnetism in the normal sate.[25] Gd^{3+}-doped ESR measurements in these compounds showed that the g shift and Korringa rate are not strongly changed by Sn substitution [see Fig. 4(a)].[12] The Gd^{3+} relaxation in these alloys is always via a single s-like conduction band and J_{fs} is q independent, decreasing slightly with increasing x (Fig. 7).[12]

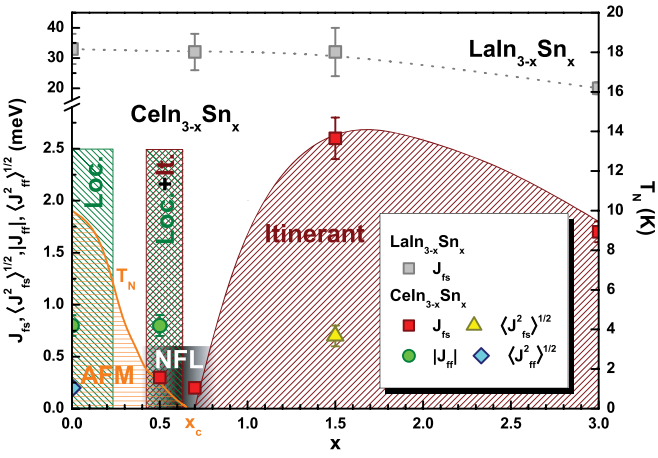

FIG. 7. (Color online) Effective exchange interaction parameter evolution as a function of Sn substitution. Data for $LaIn_{3-x}Sn_x$ compounds are taken from Ref. 12. The AFM temperature transition T_N evolution and the non-Fermi-liquid (NFL) region in the vicinity of the critical Sn concentration x_c are also shown.[5] For $CeIn_{3-x}Sn_x$ one can identify the presence of only the localized (Loc.) spin behavior for $x = 0$ and the itinerant (It.) character for $x \geqslant 0.7$, since only a single-band effective exchange interaction is probed in each case. At $x = 0.5$, near the quantum critical point, Gd^{3+} ESR probes both localized and itinerant components of the Ce $4f$ electron. Shaded areas and spline lines are guides for the eye.

For $CeIn_{3-x}Sn_x$ compounds the evolution of the Gd^{3+} ESR with Sn substitution is not as straightforward as in $LaIn_{3-x}Sn_x$. The b and Δg values change profoundly as a function of x [Fig. 4(a)]. For $CeIn_3$, as we have seen, there is no exchange interaction between Gd^{3+} and the s-like conduction electrons. This is due to the Kondo effect, which creates an attractive potential for these s-like conduction electrons at the Ce sites, reducing its density at the Gd site. In this case, the Gd^{3+} ESR relaxes only via an f-like localized band. This attests that the Ce $4f$ electrons in $CeIn_3$ are strongly localized under high Kondo screening, which also prevents the Gd^{3+} resonance from sensing the AFM transition below $T_N = 10$ K.

As the system approaches the QCP ($x = 0.5$), but still presenting AFM order, we observe the appearance of multiband effects in the resonance which are related to the delocalization of the $4f$ electrons, induced by the Sn substitution, giving rise to an s-like band. For this alloy the Ce $4f$ electrons coexist as localized and itinerant. In the vicinity of the QCP ($x = 0.7$), on the nonmagnetic side of the phase diagram, the resonance assumes a character where the relaxation is via a single s-like band. The effective exchange interaction parameter $J_{fs}(0)$ in this compound is, within experimental errors, the same as at $x = 0.5$, but no local f-like electrons are probed by the Gd^{3+}; only the itinerants.

Further increase in the Sn substitution does not alter the Gd^{3+} relaxation process, which remains being via a single s-like conduction band. For $x = 1.5$ the exchange interaction is q dependent, indicating that it is not constant over the Fermi surface and this dependance might be related to an anisotropy observed in the s-f hybridization for $CeIn_1Sn_2$.[26] In $CeSn_3$ the $J_{fs}(0)$ value decreases slightly compared to $CeIn_{1.5}Sn_{1.5}$, probably due to intermediate valence effects and/or lattice expansion. Thus, once the system crosses the QCP the hybridization of the localized $4f$ electrons with the conduction band becomes a global process and it behaves only as an itinerant.

Figure 7 qualitatively summarizes this discussion of Gd^{3+} ESR evolution in $CeIn_{3-x}Sn_x$ materials.

VI. CONCLUSIONS

For $CeIn_{3-x}Sn_x$, our conclusions are not drawn solely based on the values of the extracted or derived parameters, as a function of Sn concentration, but mostly based on the fact that one cannot analyze in the same way the Gd^{3+} ESR of each sample. When comparing the $LaIn_{3-x}Sn_x$[12] and $CeIn_{3-x}Sn_x$ systems, one can immediately realize that the evolution upon substituting In by Sn is dramatically different. While for La-based compounds only a slight change in the $J_{fs}(0)$ value is observed, for the HF one, the Gd^{3+} effective exchange parameter alters significantly, depending on the x value. However, the only difference between these systems is the addition of an $4f$ electron. So, the discrepancy in the evolutionary behavior must come from the physics of this extra $4f$ electron. For the $x = 0$ end member this additional electron is localized and highly screened by the conduction electron sea, and thus, Gd^{3+} ESR only probes an f-like localized band. However, for the other end member, $x = 3$, no local magnetism occurs and the compound can be described as an HF Landau Fermi liquid, where the Gd^{3+} resonance relaxes only via a single s-like itinerant band. On the other hand, in between, specifically for $x = 0.5$, we observe multiband effects on the ESR data, i.e., contributions of localized and itinerant bands that are originated from the same Ce extra $4f$ electron. Therefore, we argue that the microscopic evolution of the $4f$ electron in the $CeIn_{3-x}Sn_x$ system, as a function of Sn substitution, can be understood as a transition from localized to itinerant, where the localized character exists only in the AFM phase and dies out at the QCP, while the itinerant behavior can even coexist in the AFM state.

From the ESR results we observe that there are still some local moments very close to the QCP in the AFM state ($x = 0.5$) and none in its vicinity on the nonmagnetic side ($x = 0.7$) of the phase diagram. However, from our data, it is difficult to assert whether the QCP in $CeIn_{3-x}Sn_x$ is of the itinerant or the localized scenario, and further ESR experiments in samples with different Sn contents are needed to clarify this issue.

VII. SUMMARY

In summary, our ESR results microscopically show that for the $CeIn_{3-x}Sn_x$ system the AFM end member has only highly screened local moments, whereas for the nonmagnetic samples just itinerant bands are probed. For $x = 0.5$, in the vicinity of the QCP, on the AFM side of the magnetic phase diagram, the $4f$ electron has a dual character, being at the same time localized and itinerant, giving rise to multiband effects.

ACKNOWLEDGMENTS

We thank J. C. B. Monteiro and F. C. G. Gandra for their help with the polycrystalline samples. This work was supported by FAPESP (Grant Nos. 06/55347-1, 06/60440-0, 07/50986-0 and 11/01564-0); CNPq, FINEP, and CAPES (Brazil); and NSF (Grant No. NSF-DMR-0801253) (USA).

*eduardo.bittar@lnls.br

[1] G. R. Stewart, Rev. Mod. Phys. **56**, 755 (1984).
[2] H. v. Löhneysen, A. Rosch, M. Vojta, and P. Wölfle, Rev. Mod. Phys. **79**, 1015 (2007).
[3] S. Nakatsuji, S. Yeo, L. Balicas, Z. Fisk, P. Schlottmann, P. G. Pagliuso, N. O. Moreno, J. L. Sarrao, and J. D. Thompson, Phys. Rev. Lett. **89**, 106402 (2002).
[4] J. M. Lawrence, Phys. Rev. B **20**, 3770 (1979).
[5] P. Pedrazzini, M. G. Berisso, N. Caroca-Canales, M. Deppe, C. Geibel, and J. G. Sereni, Eur. Phys. J. B **38**, 445 (2004).
[6] N. D. Mathur, F. M. Grosche, S. R. Julian, I. R. Walker, D. M. Freye, R. K. W. Haselwimmer, and G. G. Lonzarich, Nature **394**, 39 (1998).
[7] N. Berry, E. M. Bittar, C. Capan, P. G. Pagliuso, and Z. Fisk, Phys. Rev. B **81**, 174413 (2010).

[8]R. Küchler, P. Gegenwart, J. Custers, O. Stockert, N. Caroca-Canales, C. Geibel, J. G. Sereni, and F. Steglich, Phys. Rev. Lett. **96**, 256403 (2006).
[9]A. V. Silhanek, T. Ebihara, N. Harrison, M. Jaime, K. Tezuka, V. Fanelli, and C. D. Batista, Phys. Rev. Lett. **96**, 206401 (2006).
[10]R. Settai *et al.*, J. Phys. Soc. Jpn. **74**, 3016 (2005).
[11]S. Kawasaki, M. Yashima, Y. Kitaoka, K. Takeda, K. Shimizu, Y. Oishi, M. Takata, T. C. Kobayashi, H. Harima, S. Araki, H. Shishido, R. Settai, and Y. Ōnuki, Phys. Rev. B **77**, 064508 (2008).
[12]E. M. Bittar, C. Adriano, C. Giles, C. Rettori, Z. Fisk, and P. G. Pagliuso, J. Phys.: Condens. Matter **23**, 455701 (2011).
[13]T. Gambke, B. Elschner, and L. L. Hirst, Phys. Rev. Lett. **40**, 1290 (1978).
[14]J. G. S. Duque, R. R. Urbano, P. A. Venegas, P. G. Pagliuso, C. Rettori, Z. Fisk, and S. B. Oseroff, Phys. Rev. B **76**, 125114 (2007), and references therein.
[15]E. M. Bittar, J. G. S. Duque, P. A. Venegas, C. Rettori, and P. G. Pagliuso, Physica B **404**, 2995 (2009).
[16]W. D. Grobman, Phys. Rev. B **5**, 2924 (1972).
[17]C. Rettori, H. M. Kim, E. P. Chock, and D. Davidov, Phys. Rev. B **10**, 1826 (1974).
[18]S. E. Barnes, Adv. Phys. **30**, 801 (1981).
[19]D. Davidov, K. Maki, R. Orbach, C. Rettori, and E. P. Chock, Solid State Commun. **12**, 621 (1973).
[20]G. E. Barberis, D. Davidov, J. P. Donoso, C. Rettori, J. F. Suassuna, and H. D. Dokter, Phys. Rev. B **19**, 5495 (1979); A. Troper and A. A. Gomes, *ibid.* **34**, 6487 (1986).
[21]Y. Yafet and V. Jaccarino, Phys. Rev. **133**, A1630 (1964).
[22]R. R. Urbano, E. M. Bittar, M. A. Pires, L. M. Ferreira, L. Bufaiçal, C. Rettori, P. G. Pagliuso, B. Magill, S. B. Oseroff, J. D. Thompson, and J. L. Sarrao, Phys. Rev. B **75**, 045107 (2007).
[23]J. W. M. Pinto and H. O. Frota, Phys. Rev. B **64**, 092404 (2001); A. Ghosh, M. S. Gusmão, and H. O. Frota, Eur. Phys. J. B (in press, 2012).
[24]T. Gambke and B. Elschner, J. de Phys. Colloques **40**, C5-331 (1979).
[25]A. M. Toxen, R. J. Gambino, and L. B. Welsh, Phys. Rev. B **8**, 90 (1973).
[26]A. P. Murani, A. Severing, M. Enderle, P. Steffens, and D. Richard, Phys. Rev. Lett. **101**, 206405 (2008).